Experimental Analysis and Semicontinuous Simluation of Multicomponent Fuel Droplet Evaporation at Low Temperatures : Proceedings 26th European Conference on Liquid Atomization & Sp...

Conference Paper · September 2014

CITATIONS
0

READS
237

5 authors, including:

Sebastian Lehmann
Sigmund Lindner GmbH
21 PUBLICATIONS **171** CITATIONS
SEE PROFILE

Etienne Rivard
Hydro-Québec
9 PUBLICATIONS **650** CITATIONS
SEE PROFILE

Sebastian Lorenz
Bundesamt für Strahlenschutz, BfS
28 PUBLICATIONS **305** CITATIONS
SEE PROFILE

Wolfgang Mühlbauer
University of Bayreuth
20 PUBLICATIONS **245** CITATIONS
SEE PROFILE

Experimental Analysis and Semicontinuous Simulation of Multicomponent Fuel Droplet Evaporation at Low Temperatures

Sebastian Lehmann*, Etienne Rivard, Sebastian Lorenz, Wolfgang Mühlbauer, Dieter Brüggemann
Chair of Engineering Thermodynamics and Transport Processes, University of Bayreuth, Germany
Bayreuth Engine Research Center (BERC), University of Bayreuth, Germany
*Corresponding author: LTTT@uni-bayreuth.de

Abstract
Fuel evaporation plays a crucial role in IC engines and other combustion devices. Their further improvement can be supported by a thorough understanding of the evaporation process. Its theoretical description is a great challenge as multi-component fuels not only may contain several hundred different chemical species with different physicochemical properties, but also defined amounts of biogenic additives, e.g. Ethanol. In this context, so called semi-continuous approaches are preferred to model the various chemical properties.
For evaporation of droplets at low ambient temperatures, a non-uniform temperature distribution inside the droplet has to be considered. Therefore a finite thermal conductivity was included in the development of a one-dimensional radial evaporation model. In the context of this study, this model was applied to the common fuel type E85, a composition of ethanol and gasoline in a ratio of 85 % / 15 % by mass. For comparison numerical simulations with infinite thermal and mass diffusivity models were conducted.
A detailed analysis of evaporating E85 and surrogate fuel droplets over a wide range of initial droplet diameters and ambient temperatures is presented here. For an elaborate validation of numerically predicted diameter decrease and composition change, two relatively simple but yet precise experimental setups have been developed. The first method utilizes a sensitive weighing technique, where droplets in a diameter range from 70 to 150 µm of a droplet chain are collected by a high precision scale after different falling times. Accurate average diameter values can be determined by a simultaneous evaluation of mass increase. Subsequently a gas chromatographic analysis of the composition of the droplets was conducted. In the second experiment evaporation of even smaller single E85 droplets was optically analysed by a high-speed shadowgraphy/schlieren microscope setup. The successful comparison of experimental and numerical results shows the applicability of the developed model over a large range of diameters and temperatures.

Introduction

Fuel atomization and evaporation plays a crucial role in the operation of IC engines and other combustion devices. Especially in the field of IC engines, the ongoing developments in modern injection systems are aimed at to reach an efficient and engine-operating matched atomization and thus evaporation of liquid fuel. Current systems favor direct injection with high pressures to achieve smaller droplets and high evaporation rates [1]. To guarantee an efficient and low-pollutant combustion, a balanced gaseous mixture of fuel and oxidizer is required, too. This necessitates a thorough understanding of the underlying droplet evaporation processes to allow further engine optimization.
Many fuels like gasoline consist of several hundred chemical species, which has a great influence on the individual evaporation properties of each fuel. Additionally, fuels worldwide are more and more supplemented by biogenic fuel blends not only for ecological reasons [2], [3].
To understand the rather complex multicomponent fuel droplet evaporation processes, a considerable amount of basic numerical and experimental work has been conducted in the recent years, e. g. [4], [5]. A great challenge represents the numerical modeling of these multicomponent mixtures of a discrete component like ethanol with a rather complex chemical composition as is e. g. gasoline. It is a general consideration in simulation purposes to strike a balance between accuracy and calculation time [6]. Earliest models, as the well-known d^2-law rely on constant droplet temperature and composition and so require relatively low computational effort. More accurate models are able to consider to varying degrees the internal mixing in multicomponent droplets up to the full solution of the Navier-Stokes-equation but then often demand unreasonable resources for application-related cases. A way widely approved to address this defiance is the application of “semi-continuous” models. They combine the well-established description of physicochemically similar species by continuous distribution functions with a discrete component modeling

(e. g. [7]). So not only each different component or component group can be treated appropriately to their characteristics but also a reduction in computing time is achieved.
A wide-spread approach is the inclusion of mass diffusion which considers the gradient of the concentrations of the components in the droplet. The latter one is a result of the different evaporation of different components. However, an additional gradient of temperature which will be formed due to heat exchange and evaporation at the surface has often been neglected by other authors under the assumption that heat diffusion is several orders of magnitude faster than mass diffusion [8], [9]. While this holds for higher temperatures, heat diffusion has to be taken into account as the temperature decreases. By employing a finite heat diffusion rate in a numerical simulation, the differences in the varied modeling approaches have already been published [10]. Recent publications also show these deviations between modeling and experimental data especially for the lowest examined temperatures [11].
The experimental validations of droplet evaporation models mainly rely on optical approaches. Larger droplets (> 100 µm), free falling or suspended to e. g. glass fibers, are often surveyed by macro-objective photography or video recording [12]. The velocity and diameter decreases of droplets less than 100 µm is frequently determined by laser-based methods. Wide spread methods include PDA- and LDA-measurements, but also holography is employed [13], [14]. Temperature and composition examinations require more complex techniques [15].
In this work E85 as a worldwide employed fuel type was chosen to examine the global influence of the temperature gradient at low ambient temperatures and validate the developed model. Two alternative experimental setups have been developed. The first method is based on calculating the evaporation rate from the decrease in weight of several hundred thousands of droplets after a defined falling distance. The second method relies on the optical determination of the decrease of droplet diameter with a combined shadowgraphy/schlieren microscope. Both setups are relatively simple and inexpensive to realize but yet deliver precise results of droplet diameter and velocity decrease. Another advantage is the possibility for a gas chromatographic analysis of the collected droplets which yields the determination of an averaged droplet composition. A detailed analysis of diameter decrease and composition change of droplets of E85 and alkane mixtures has been conducted over a wide range of initial droplet diameters and temperatures and compared to the numerical predictions.

Numerical model

The model is aimed at simulations of droplet evaporation for mixtures of complex substances containing very large numbers of chemical species such as gasoline and discrete treatable components, like ethanol. Therefore an approach is chosen, which utilizes *j* discrete components with each component being either a pure substance or a continuous mixture. The mole fraction *x* of a single species *i* as part of a continuous mixture then becomes

$$x_i = x_j f_j(I)\Delta I \tag{1}$$

I represents the molar mass of the species and f the distribution function. The relative fractions of the species are expressed by the statistics of the distribution that are functions of the parameters themselves. For comparison, also mixtures of pure substances can be modelled. The rates of vaporization and heat exchange with the surrounding air are calculated according to the quasi-steady “film theory” of Abramzon and Sirigano [16]. The vaporization rate is given by the following explicit expression

$$\dot{n} = 2\pi \bar{c}_g \bar{D}_{v,g} r_s Sh^* \ln(1 + B_n) \tag{2}$$

where $\bar{c}_g$ is the average molar density of the gas phase, $\bar{D}_{v,g}$ is the average diffusivity of the vapour in the surrounding gas phase, r_s is the radius of the droplet, Sh^* is the modified Sherwood number and B_n is the Spalding molar transfer number. The energy balance of the droplet is calculated from a control volume defined by the surface of the droplet. Vapour-liquid heat transfer is the result of two contributions: energy needed for evaporation and heat exchange with the surrounding gas. The heat flow is calculated with the expression

$$\dot{Q} = \dot{n}\bar{\bar{C}}_{p,v}(T_\infty - T_s)B_h^{-1} - \dot{n}\Delta H_{v,l,s} \tag{3}$$

where $\dot{n}$ is the molar flow rate, $\bar{\bar{C}}_{p,v}$ is the average molar specific heat capacity of the vapour phase, T_∞ is the temperature of the gas phase at an infinite distance of the droplet, T_s is the surface temperature, B_h is the Spalding heat transfer number and $\Delta H_{v,l,s}$ is the enthalpy of vaporization of the liquid phase at the droplet surface. The Spalding heat transfer number is calculated with the method suggested by Abramzon and Sirignano [16] for temperatures remaining below the boiling point of the mixture. When the surface temperature exceeds the boiling point, heat and mass flow is calculated with a different approach [17]. Heat and mass transfer equation becomes

$$\dot{n}\Delta H_{v,l,s} = \dot{Q}_i - \dot{Q}_o \tag{4}$$

where $\dot{Q}_i$ is the rate of heat transfer from the inside of the droplet and $\dot{Q}_o$ is the heat transfer in the opposite direction. $\dot{Q}_i$ and the associated heat transfer enhancement coefficients are evaluated with the method of Adachi et al. [18]. $\dot{Q}_o$ is expressed as

$$\dot{Q}_o = \kappa \bar{\bar{C}}_{p,g,s}\dot{n} \cdot \exp\left(-\frac{2r_s \bar{C}_{p,g,s}\dot{n}}{kNu}\right)(T_\infty - T_b) \tag{5}$$

where the correlation factor κ is set to 2.0 [17]. $\bar{\bar{C}}_{p,g,s}$ is the average molar specific heat capacity of the gas phase at the surface, Nu represents the Nusselt number of the droplet. The vapour-liquid equilibrium used to evaluate the properties of the gas phase is Raoult's law. It is also assumed that the liquid and gas temperatures at the surface of the droplet are at equilibrium.

The velocity of the droplet is calculated under the assumption that the droplet follows a one-dimensional trajectory parallel to the gas flow. Acceleration then is

$$\frac{\mathrm{d}v_{rel}}{\mathrm{d}t} = \frac{\sum F}{m_d(t)} \tag{6}$$

where v_{rel} is the relative velocity of the droplet, $\sum F$ summarizes the forces acting upon the droplet and $m_d(t)$ is the mass of the droplet as a function of time. Three main forces are acting on the droplet: gravitation, buoyancy and drag. Drag is calculated with the classic Rayleigh equation

$$F_d = -0.5 * \rho_f v_{rel}^2 A c_d \tag{7}$$

where F_d is the drag force, ρ_f is the mass density of the flow, v_{rel} is the relative velocity of the droplet, A is the orthographic projection of the droplet on a plane perpendicular to the direction of motion. Subscript f stands for flow and designates the mixture in transit from the liquid phase to the gas phase which has a composition that is different from these two phases. The drag coefficient c_d is calculated with the relations of Yuen and Chen [19], Clift et al. [20] and Renksizbulut and Yuen [21].

Within this framework droplet evaporation is simulated under different combinations of assumptions regarding diffusivity and thermal conductivity.

Low-temperature effects on evaporation are especially considered by modelling composition and temperature as one-dimensional radial fields in the so called diffusion-limited (DL) case. This represents a particularity of the model presented herein because temperature is often assumed to be uniform in the droplet because of the high rate of heat diffusivity when compared to mass diffusivity [9]. Supplementary, a hybrid (HY) model consisting of diffusion-limited mass transfer and infinite thermal conductivity and a well-mixed (WM) model assuming uniform composition and temperature are generated for comparison.

For HY and DL models the mass transfer inside the droplet is calculated by

$$\frac{\partial}{\partial t}\left(c_l x_{l,i}\right) = \nabla \cdot \left(c_l \chi D_{l,i,m} \nabla x_{l,i}\right) \tag{8}$$

where c_l is the molar density of the liquid phase, $x_{l,i}$ is the molar fraction of a single species in the liquid, χ is the internal recirculation factor suggested by Abramzon and Sirigano [16] to approximate the effect of convection inside the droplet and $D_{l,i,m}$ is the diffusivity of a species. Equations for the parameters of the distribution are obtained by substitution of Eq. (1) in (8) and integration over *I*. To specifically account for the influence of low temperatures in the DL-model, a similar diffusion equation is implemented for heat transfer:

$$\frac{\partial}{\partial t}\left(c_l C_{p,l} T_l\right) = \nabla \cdot \left(\chi k_l \nabla T_l\right) \tag{9}$$

Here $C_{p,l}$ is the molar specific heat capacity of the liquid phase, T_l the liquid temperature and k_l the thermal conductivity of the liquid phase. The rate of recession of the droplet radius r_s with time t is calculated by the ordinary differential equation

$$\frac{dr_s}{dt} = -\frac{1}{c_l}\left(\frac{\dot{n}}{4\pi r_s^2} + \frac{r_s}{3}\frac{dc_l}{dt}\right) \tag{10}$$

The WM model with its assumption of infinite mass or thermal diffusivity employs the following equations for the concentration of a species and the temperature of the liquid phase:

$$\dot{x}_{l,i} = \dot{n}\left(x_{l,i} - x_{f,i}\right)/n_d \tag{11}$$

$$\dot{T}_l = \dot{Q}/(n_d C_{p,l}) \tag{12}$$

Variable n_d represents the fraction of substance in the droplet.
A more detailed description of the developed semicontinuous multicomponent (SCMC) model and the obtained numerical results can be found in the work of Rivard and Brüggemann [10].

Experimental setups

In order to experimentally achieve evidence of the predictions of the developed simulation, velocities and diameter decreases as well as composition change of different droplets after different falling times have to be determined for low ambient temperatures. To allow investigations over a wide range of initial droplet diameters and associated velocities, two different droplet generators have been employed.
The first system is based on breaking up a laminar jet by a vibrating orifice by specific disturbances in a monodisperse stream of droplets (MDG-100, TSI Inc.). The primary droplet diameter is a function of volume flow and frequency [22], whereupon frequency depends on density, viscosity and surface tension of the applied fluid [4]. The utilization of a highly accurate frequency generator (HM 8131-2, HAMEG) as well as a precise syringe pump (KDS-100 CE, kd Scientific) to control volume flow allows the primary droplet diameter to be calculated with a negligible error. Equally the initial droplet velocity can be calculated from the volume flow of the stream because of momentum conservation while the stream breaks up. As simulation requires droplet initial diameter and starting velocity as input parameters, these sizes thus can be determined independently from any setup.
In the second system, single droplets have been generated by applying voltage pulses of different lengths and amplitudes to a small fluid reservoir (PicPIP, Gesim mbH). Different pulse settings result in different droplet sizes and velocities for different liquids, which have to be characterized separately. By changing the repetition rate, droplets in a frequency range up to 1000 Hz can be provided, as well as single droplets.
These different ways of generating droplets lead to the development of two relatively simple but yet precise experimental setups for determination of droplet diameter and velocity. Besides a rather inexpensive realization, they further offer the advantage to collect the examined droplets for later gas chromatographic composition analysis, so that all quantities to be measured can be taken at once.
As the droplet generation rate for the MDG-100 lies in the range of several kHz, a sensitive weighing-technique was utilized. It combines the possibility of collecting the droplets at different points of their trajectory for a later gas chromatography with a simultaneously automated droplet mass determination (Fig. 1). To guarantee a high weighing accuracy, an electronic scale with a precision of 0.2 mg was employed. The scale was connected to a data acquisition system that takes a reading every 0.5 second. In that time several hundred thousand droplets steadily increase the weight. To guarantee a stable operation of the droplet generator, different measures were taken. This includes particularly the utilization of a small-porous filter in the feed line to prevent clogging of the orifice and the general cleaning of the system after each measurement. Additionally, a program was developed which collects weight data and monitors the constant increase of mass in real time by calculating a regression line. If deviations from the slope exceed a pre-defined value, the series of measurements is stopped and rejected if there are not enough data points. By means of this method, sources of errors which normally would not be observable in the course of measurement, would lead to small deviations from the linear increase in mass and thus can be detected and avoided. These errors may be unsteady droplet coagulation in the droplet chain enforced by e.g. fluctuations in the ambient air or a not constant initial droplet temperature due to heating-up of the fuel by thermal heat transfer between heating chamber and droplet generator. The occurrence of static charge was minimized by grounding the individual setup components. Further measures like employing deionized air are found not to be necessary. Due to the mentioned measures, very high accuracy could be achieved. Consequently, a good experimental validation of the simulation can be conducted by relative simple means.
In order to obtain data for droplet evaporation also at elevated ambient temperature, a heating chamber surrounding the droplet chain was implemented. A uniform temperature field is obtained by heatable top and bottom disc. To keep low initial droplet temperatures, heat transfer to the MDG-100 is prevented by an appropriate insulation. Different falling heights are realized by varying the distance between the plates.

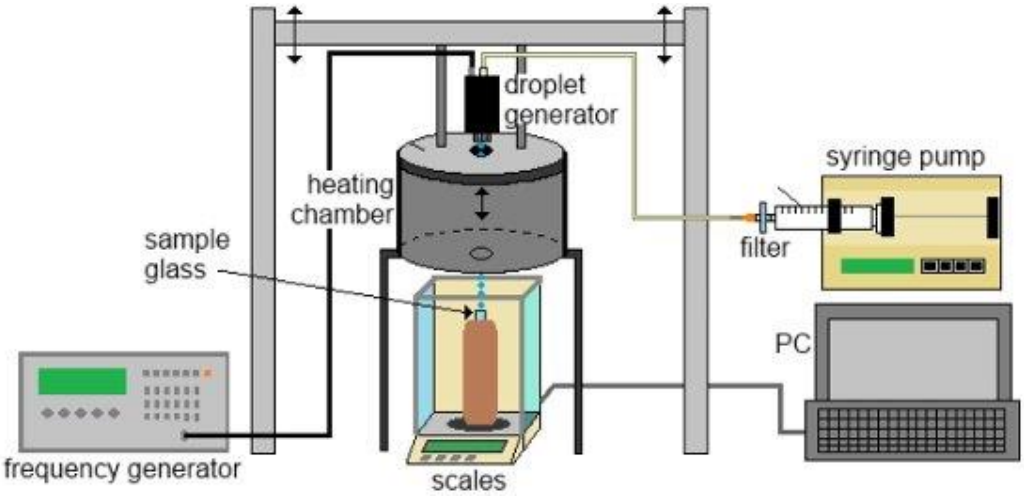

Fig. 1. Experimental setup for analyzing droplet evaporation by means of an advanced weighing method at different ambient temperatures.

The developed model is based on the surface model of Sirignano [4] which accounts for a general concentration of fuel vapor in the environment. For the simulations it is assumed that this environmental concentration is zero. Hence, an adversely affected evaporation by a saturated chamber atmosphere has to be excluded. Supported by steady-state CFD calculations of the radial and axial distribution of vapor for a high rate steady chain of volatile n-pentane droplets at maximal ambient temperature of 363 K (Fig. 2), the chamber size was configured adequately.

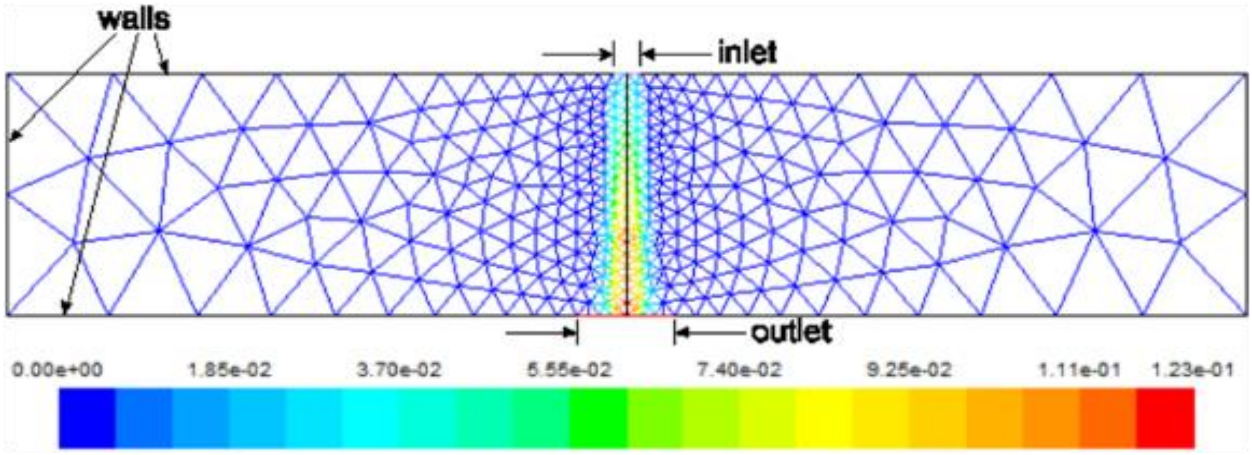

Fig. 2. Simulation of vapour concentration for evaporating n-pentane in the employed heating chamber.

While the extent of the vapor “cloud” remains very limited for the chosen design and thus negligible in radial direction, strong evaporation takes place in axial direction as droplet mass decreases by slightly less than 48 %. Nonetheless, the concentration in the ambient air amounts to less than 10 % even for the shown conditions. Consequently, the concentration gradient along the droplet chain can be neglected for experiments with E85 and a decreased droplet rate. The decreased rate also accommodates the fact that droplet interactions play an important role in evaporation and later combustion [23]. An explicit example for droplet chains is presented by Fieberg et al. [24], who show a modification of drag and Reynolds number for droplet distances smaller than ten times of the droplet radius. In this work, an enhanced droplet distance was set by choosing appropriate parameters of frequency and volume flow. The assumption of droplets in an ideally flow with negligible interactions between single droplets thus can be justified.

Sets of appropriate parameters for uniform droplet generation with sufficient distance between the droplets and without satellite droplets and coagulation in the measurement distance were determined optically for E85 and mixtures of alkanes. High optical transmission values of the tested fluids had to be taken into account. Inspired by Settles [25], a setup combining shadowgraphy and schlieren technique with a proper magnification was developed. By utilizing a high-speed camera with short exposure time for simultaneous recording of the droplet size and movement, a high-speed shadowgraphy/schlieren setup was established (left part of Fig. 3). Considering the possible generation parameters for

the MDG-100 to avoid droplet interaction as well as the sensitivity of the employed scale, stable droplet chains within an initial droplet diameter range of 70 to 150 µm could be identified and properly examined by the weighing technique.

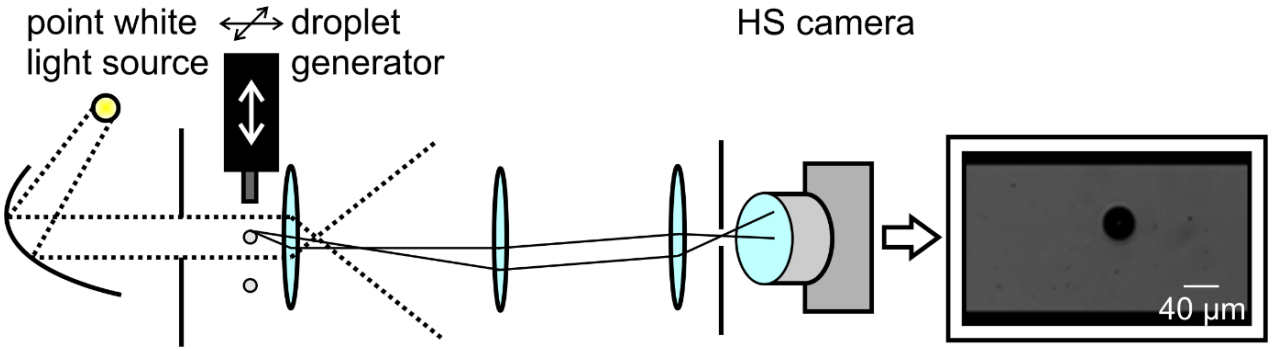

Fig. 3. Experimental setup for optically analysing single droplets with diameters less than 70 µm.

As application-oriented diameters for the evaporation of fuels lie within diameter ranges of several 10 µm, it is desirable to further minimize the accessible size region by maintaining the requirements already discussed. For this application range, the second droplet generator PicPIP is utilized. As for the smaller droplets the decrease in mass cannot be resolved by weighing method, the high-speed shadowgraphy/schlieren setup was further refined by appropriate magnifying optics to become a high-speed shadowgraphy/schlieren microscope (Fig. 3). Thus, droplet diameter and velocity decrease can be observed directly.

A plasma white light source (EQ-99-FC LDLS, Energetiq Technology Inc) along with a 220 µm optical output light guide is used as high quality point light source. The rays of the light source are parallelized. Part of the illuminated droplet trajectory is then magnified by the internally assembled microscope to the high-speed camera. The droplets refraction index bends the parallelized light in such a way that the droplets are imaged clearly enlarged with good contrast to the bright background. The excellent illumination further allows short exposure times below 5 µs. Thus, sharp images with high dynamical range can easily be accomplished over a wide range of initial droplet velocities. Different points of the trajectory can be observed as the droplet generator is mounted maneuverable. For the PicPip-generator no relation is given to calculate the droplet diameter as it was possible for the MDG-100. So no direct relation between recorded pixel size and actual size of the droplet can be obtained. This issue was addressed by calibrating the optical system with a stage micrometre. Besides, the calculated droplet size of the MDG-100 serves as an independent source of validation for the quality of this calibration.

By applying an object recognition algorithm in Matlab®, droplet positions and diameters can be reproducibly evaluated in the recorded videos. Therefore an automated evaluation by statistical means and constant recognition parameters is guaranteed over the whole measurement range.

Under consideration of the aforementioned arguments, a second size-adjusted heating chamber was designed for the microscope setup. Accommodating to the smaller droplet sizes, a smaller temperature range from 293 to 310 K is accessible.

In summary, droplets of E85 and different alkane-mixtures within a diameter range of 40 to 150 µm and velocity range of 1 to 9 m/s in an ambient temperature range from 293 to 350 K could be precisely examined. This allowed to gain a high load of experimental data over a widely varied range of parameters to take account for the influence of a finite thermal heat diffusion in droplets of different fuels.

Results and Discussion

As described in section 3, the developed optical setup has been applied to determine and to optimize the parameters of the monodisperse droplet generator MDG-100 as well as the PicPIP to assure the quality of the droplet chains and droplets of different fluids. Consequently poor settings, which may result in droplets coagulating during the fall or satellite droplets, can be easily excluded. Moreover, a broad set of parameters for a stable operation of the droplet generators for E85 as practically applied fuel as well as several mixtures of alkanes can be identified rather quickly. The latter ones are mixtures of low and high boiling components, e. g. pentane, hexane and octane. They approximately represent essential components of gasoline's chemistry and thus serve as model fluids to understand evaporation behavior.

Optimal sets of parameters for both devices lead to reproducable droplet generation with very high precision, as less than 2.5% variation in diameter were observable in routine operation. Results of E85 droplet initial diameter for both droplet generators gained via the shadowgraphy/schlieren-setup are exemplarily presented in Fig. 4. Because of the higher generation rate, an almost perfect Gaussian distribution is reached for the MDG-100. But also the distribution of

the droplets of the PicPip can be considered nearly Gaussian. So the determined standard deviation in an experimental cycle for the PicPip is 0.9%, respectively 2.4% for the MDG-100.

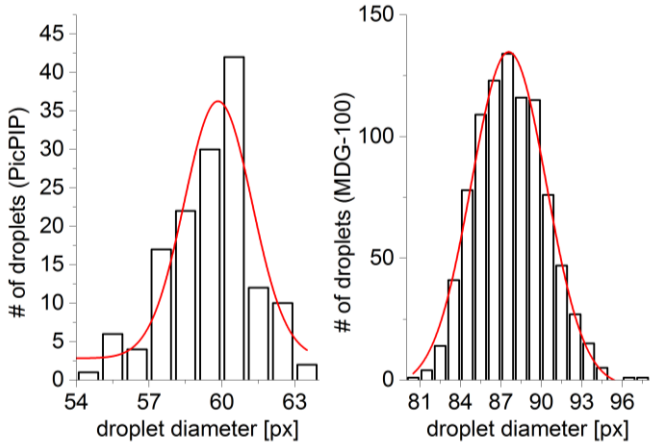

Fig. 4. Optically determined distribution of E85 droplet diameters in pixel for the PicPIP (left, pulse width 27 µs, amplitude 52 V) and the MDG-100 (right, volume flow 30 ml/h, frequency 4.33 kHz).

Optical measurements were conducted at several distances below the particular nozzles. In order to compare the experimentally gathered data to the numerical results, a precise rescaling of the falling distance into a falling time has to be performed. As droplet motion is recorded by a high-speed camera with high frame rate (8000 fps), single droplets can be traced over multiple frames. Each covered distance is then calculated by determining the droplet positions frame by frame with the described object recognition algorithm. Assuming constant velocity over the camera-given small timespan between two images, droplet velocity now can be simply calculated. The results for different initial velocities are compared to the numerically calculated velocities, as shown in Fig. 5. A very good agreement between model and data could be reassured. Consequently, the numerically calculated velocity decrease is utilized for a conversion from falling distances into falling time in the following.

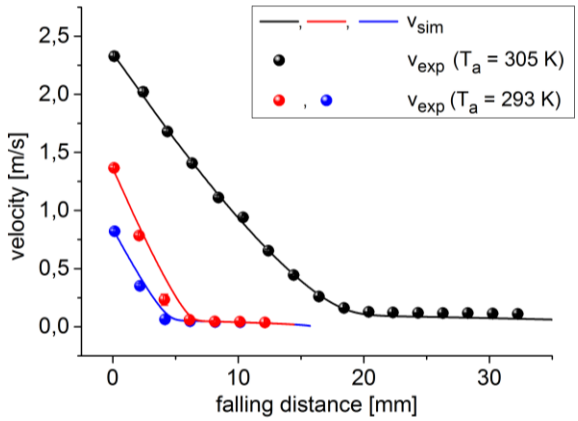

Fig. 5. Comparison of modelled and measured velocity decrease for different droplet initial velocities at different ambient temperatures.

After calibrating the optical setup and the time axis, the diameter decrease of droplets of E85 and different mixtures of alkanes have been measured over several falling distances and ambient temperatures with the introduced methods to validate the numerical model.

In the context of a sufficient and constant fall distance between the droplets without coagulation, two pairs of parameters were selected for the MDG-100. A minimal initial diameter of 72.5 µm is possible at normal ambient temperature of 293 K. To enhance evaporation rate and determine the effect of heat transfer also for higher ambient temperatures the chamber has been heated up to 350 K. However, this influences the stability of the droplet chain, so that droplet size and velocity also has to be enlarged. For a maximum chamber temperature of 350 K, a sufficient droplet chain with initial radius of 153 µm could be identified. Since heat flow between chamber and MDG-100 is suppressed by insulation

of the upper heated plate, the initial temperature of the droplets at the nozzle is supposed to equal room temperature (294 K). With the above described real time analysis of the scale data, this assumption is proved over the whole measurement time. For that reason accurate measurement at well-defined parameters is guaranteed.
The determined diameter decrease of E85 droplets with initial radius of 72.5 µm and 153 µm is presented in Fig. 6. As initial droplet velocity has to be increased for the bigger droplets, data collection is limited to two measurement points for the available chamber size. The error bars in time are calculated with the variances in optical droplet velocity determination. Statistical spread of droplet diameters is indicated by the error bars of the diameter. Results of the numerical analysis are visualized in Fig. 6 as lines. The dash-dotted line symbolizes the WM-model; the dashed one stands for the HY-model while the solid line represents the DL case. The differences within the models have already been discussed in a previous paper [10]. The consideration of a finite heat transfer in DL model leads to a slowing down of evaporation and thus diameter decrease, which is supported by both sets of experimental data. Deviations to the DL model is only observable at the end of the timescale for the smaller droplets. This is due to the fact that droplet velocity becomes so low that droplet coagulation due to disturbances of the surrounding air cannot be excluded anymore. Despite the high sensitivity of the scale and the implemented error interception, this constant source of error leads to a linear increase in mass. Droplet evaporation thus becomes underestimated at the end of the measurement range. Apart from that the accordance between the experimental data and the calculated diffusion-limited model is obvious.
The introduced weighing technique thus allows a precise determination even of small changes in droplet diameter via the scales over a wide range of parameters. Differences in a percent range can be detected reliably. Even if the temperature of the surrounding chamber exceeds the initial temperature by almost 60 K, what can already be denoted as elevated temperature in terms of the model assumptions, it can be clearly seen that the influence of heat diffusion cannot be neglected. Already in the first few time steps in our arrangement, evaporation is found to be slower than predicted by the widespread WM-model.

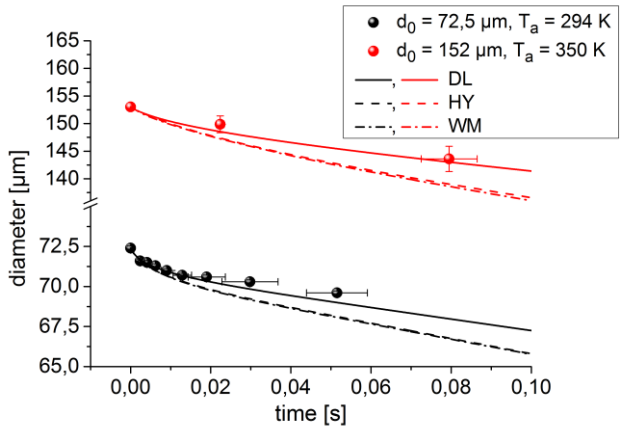

Fig. 6. Evaporation of E85 droplets: Comparison of experimental data measured with advanced weighing method and simulated data for different ambient temperatures.

Additionally, the droplets respectively droplet chains were collected in a sample glass in order to analyse the change in composition by gas chromatography. To reduce evaporation losses and the momentum transfer to the scale, a solvent was utilized to pick up the droplets during the experiments. Furthermore this has the advantage that an internal standard can be intermixed with the solvent. Thus, a precise calibration of the gas chromatographic system is enabled which leads to comparative and reproducible results of composition change over different falling heights. As the numerical simulation models E85 as a two-component mixture, the fractions of discrete ethanol and continuous gasoline sum up to one. Hence, only the clearly detectable ethanol mass area peak has to be measured by gas chromatography. The averaged gasoline fraction of the already presented E85 droplets over several falling distances are presented in the left side of Fig. 7. Error bars in time are again derived from the variances in optical droplet velocity determination. The deviations in molar fraction for the MDG-100 are a result of combined uncertainties from the weighing technique and the gas chromatographic analysis. Especially the pronounced strong decrease of gasoline at the beginning of evaporation could be verified clearly. This indicates a quick evaporation of the light boiling components, while at later time evaporation is slowed down. In order to underline the observed behaviour of E85, additional experiments were conducted with different mixtures of alkanes. For the MDG-100, exemplarily the light boiling components are represented by pentane and hexane, while slow boiling components are substituted by heptane and octane, each component by 25 Vol.-%. Some small differences in the initial values are expectable due to impurities in the mixture

and analysis process. Gas chromatography of droplet chains with initial diameter of 77 µm reveals the expected high decrease in pentane-fraction after 0.05 s falling time, while the slow boiling components stay rather unchanged (Fig. 7, on the right).

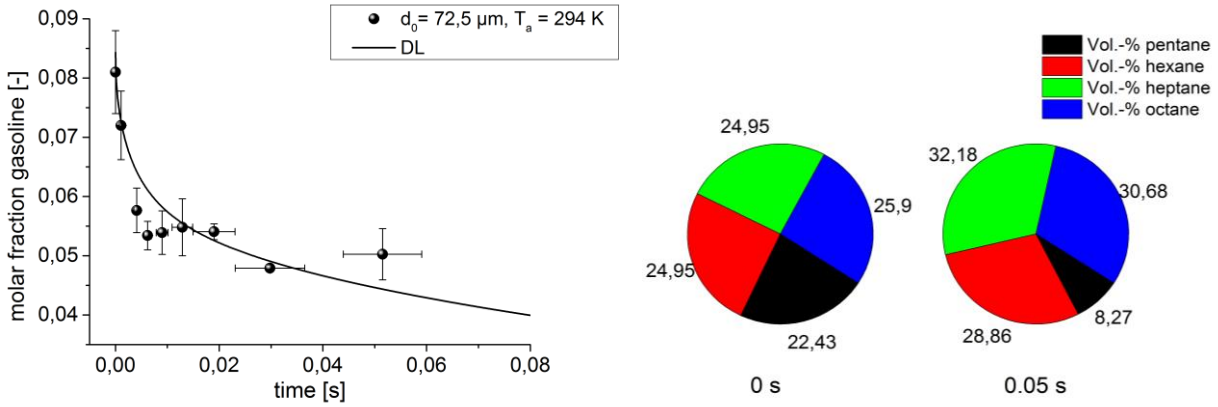

Fig. 7. Gas chromatographic analysis of collected MDG-100 droplets. On the left side the average composition change of E85 (d_0 = 72.5 µm) over the full falling height is shown, while on the right side exemplarily the initial and end composition of a $C_5C_6C_7C_8$-mixture is presented.

To further extend the numerical validation, especially for yet smaller droplet diameters, the MDG-100 was replaced by the PicPIP droplet generator. Compared to the MDG-100, the generated droplets are now too small for the introduced weighing method. Therefore, besides the finding of optimal generation parameters and velocity for axis-conversion, the droplet diameters at the different falling distances were also determined optically. A statistical analysis over several droplets per falling time is conducted by employing an object-recognition algorithm. The results of the averaged decrease of several initial droplet diameters over time are shown in Fig. 8 for ambient temperatures of 293 K and 305 K. All data points are subject to only small deviations as can be seen by the indicated error bar. The error bars in time are calculated with the variances in optical droplet velocity determination.The small deviations in flight time for the different data points are once more mainly a result of the variances in optical droplet velocity determination. Numerically calculated diameter decreases for the experimentally determined initial parameters are represented as lines in Fig. 8. As described above, the dash-dotted line symbolizes the WM model, the dashed one stands for the HY model while the solid line again represents the diffusion-limited case (DL).

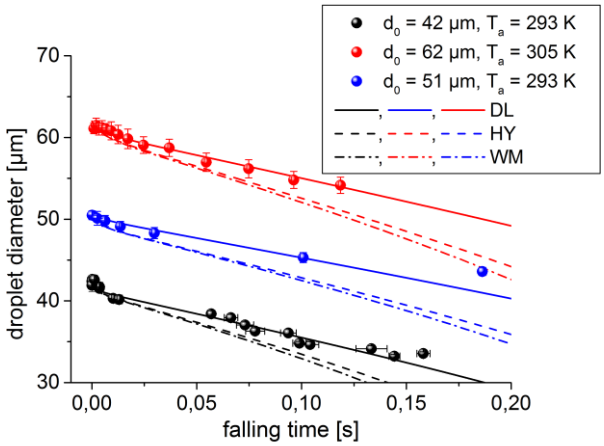

Fig. 8. Evaporation of E85 droplets: Comparison of experimental data measured with shadow/schlieren high-speed cinematography and simulated data for different ambient temperatures.

As the possible observation time with the second setup is enlarged nearly up to a factor of 7, the differences between the models increase considerably with advanced falling time. The consideration of a finite thermal diffusivity clearly tends towards a slower evaporation. There are differences between the well-mixed and combined approaches as well,

but not that distinct. As already seen in Fig. 6, deviations between experimental data and numerical model are mainly observed at the end of the particular timescale for each measurement. This is due to the fact, that at the end of the trajectory droplet velocity is so slow, that even smallest air disturbances influence the motion of the droplets. They are for example driven out of focal plane, so that the then blurry image of the droplet is misinterpreted in size by the recognition algorithm. Nevertheless the merely optically gathered data again meet very well the prediction of the numerical model that a finite heat transfer has to be included over the examined temperature range.
By employing the optical shadowgraphy/schlieren technique, the accessible range of detection was thus clearly expanded and allowed validation of the numerical predictions to still smaller droplet diameters. Again differences in a percent range can be detected reliably.

Conclusions

Three evaporation models based on semi-continuous thermodynamics with different numerical approaches for heat and mass diffusion were applied to small falling droplets of E85 and alkane mixtures. In order to survey the evaporation of the droplets at low temperatures, two different experimental setups were developed. The first one monitors the decrease in mass of a constant stream of droplets at different ambient temperatures using a highly precise digital scale at different heights after droplet generation. External influences like unwanted changes in initial droplet temperature could be effectively detected by real time analyzing the scale data. In the second setup, a combined high-speed shadowgraphy/schlieren microscope measurement technique was applied in conjunction with a single droplet generator to record the decrease of diameter of smaller droplets over a larger time span and ambient temperature of 293 to 305 K. The validity of the advanced diffusion-limited model considering a finite heat diffusivity is confirmed within the experimental errors for the evaporation of multicomponent droplets at low temperatures. The model also provides predictions of the change in droplet compositions which could be proved by gas chromatographic measurements. The observed behavior for E85 droplets is underlined by basic examinations of alkane mixtures, which approximately reflect the different fuel ingredients.
Further work will include Raman spectroscopy of the gas phase after different falling times in order to expand the possibilities of an in-situ concentration measurement technique. To address the droplet velocity change, a modification in the observation chamber regarding a supportive laminar airstream of defined velocity is pursued.

Acknowledgements

The authors are grateful for the financial support of the German Research Foundation (DFG) under grant no. BR 1713/10.

Nomenclature

A	orthographic projection of the droplet on a plane perpendicular to the direction of motion, [m²]
B_n, B_h	Spalding molar transfer number, Spalding heat transfer number, [-]
c_d	drag coefficient, [-]
$\bar{c}_g, c_l$	average molar density of the gas phase, molar density of the liquid phase, [mol m^{-3}]
$C_{p,l}$	molar specific heat capacity of the liquid phase, [J mol^{-1} K^{-1}]
$\bar{\bar{C}}_{p,g,s}$	average molar specific heat capacity of the gas phase at the surface, [J mol^{-1} K^{-1}]
$\bar{\bar{C}}_{p,v}$	average molar specific heat capacity of the vapour phase, [J mol^{-1} K^{-1}]
d_0	initial droplet diameter
$D_{l,i,m}$	diffusivity of a species, [m² s^{-1}]
$\bar{D}_{v,g}$	average vapour diffusivity in the surrounding gas phase, [m² s^{-1}]
f	distribution function, [-]
$F_{(D)}$	(drag) force, [N]
$\Delta H_{v,l,s}$	enthalpy of vaporization of the liquid phase at the droplet surface [J mol^{-1}]
I	molar mass of a species, [kg mol^{-1}]
k_l	liquid thermal conductivity, [W m^{-1} K^{-1}]
m_d	droplet mass, [kg]
n_d	fraction of substance in the droplet, [mol]
$\dot{n}$	molar flow rate, [mol s^{-1}]
Nu	Nusselt number, [-]
$\dot{Q}, \dot{Q}_i, \dot{Q}_o$	heat flow, heat flow from the inside/outside of the droplet, [J s^{-1}]
r_s	droplet radius, [m]

Sh^*	modified Sherwood number, [-]
t	time, [s]
T_a, T_l, T_s, T_∞	ambient temperature, liquid temperature, droplet surface temperature, gas phase temperature in infinite distance, [K]
v_{rel}	relative velocity of the droplet, [m s^{-1}]
$x_{(l,)i}$	(liquid) molar fraction of species i, [-]
κ	correlation factor, [-]
ρ_f	mass density of the flow, [kg m^{-3}]
χ	internal recirculation factor, [-]

DL	diffusion-limited
HY	hybrid
WM	well-mixed

References

[1] Drake, M., and Haworth, D., 2007, Proceedings of the Combustion Institute, 31(1), pp. 99–124.

[2] Stan, C., Troeger, R., Guenther, S., Stanciu, A., Martorano, L., Tarantino, C., and Lensi, R., 2001, SAE Technical Paper 2001-01-1207

[3] Sarathy, S. M., Oßwald, P., Hansen, N., and Kohse-Höinghaus, K., 2014, Progress in Energy and Combustion Science.

[4] Sirignano, W. A., 2010, "Fluid dynamics and transport of droplets and sprays."

[5] Sazhin, S., Elwardany, A., Krutitskii, P., Deprédurand, V., Castanet, G., Lemoine, F., Sazhina, E., and Heikal, M., 2011, International Journal of Thermal Sciences, 50(7), pp. 1164–1180.

[6] Sazhin, S. S., 2006, Progress in Energy and Combustion Science, 32(2), pp. 162–214.

[7] Yang, S., Ra, Y., Reitz, R. D., VanDerWege, B., and Yi, J., 2010, Atomization and Sprays, 20(11), pp. 965–981.

[8] Tamin, J., and Hallett, W. L., 1995, Chemical Engineering Science, 50(18), pp. 2933–2942.

[9] Abdel-Qader, Z., and Hallett, W. L., 2005, Chemical Engineering Science, 60(6), pp. 1629–1640.

[10] Rivard, E., and Brüggemann, D., 2010, Chemical Engineering Science, 65(18), pp. 5137–5145.

[11] Hallett, W., and Beauchamp-Kiss, S., 2010, Fuel, 89(9), pp. 2496–2504.

[12] Hallett, W., and Legault, N., 2011, Fuel, 90(3), pp. 1221–1228.

[13] Nguyen, D., Honnery, D., and Soria, J., 2011, Experiments in Fluids, 50(4), pp. 949–959.

[14] Calvo, E., García, J. A., Santolaya, J. L., García, I., and Aísa, L., 2012, Measurement Science and Technology, 23(5), p. 55202.

[15] Lemoine, F., and Castanet, G., 2013, Experiments in Fluids, 54(7), 1572.

[16] Abramzon, B., and Sirignano, W., 1989, International Journal of Heat and Mass Transfer, 32(9), pp. 1605–1618.

[17] Ra, Y., and Reitz, R. D., 2009, International Journal of Multiphase Flow, 35(2), pp. 101–117.

[18] Adachi, M., McDonell, V. G., Tanaka, D., Senda, J., and Fujimoto, H., 1997, SAE Technical Paper 970871.

[19] Yuen, M. C., and Chen, L. W., 1976, Combustion Science and Technology, 14(4-6), pp. 147–154.

[20] Clift, R., Grace, J. R., and Weber, M. E., 1978, "Bubbles, drops, and particles."

[21] Renksizbulut, M., and Yuen, M. C., 1983, Journal of Heat Transfer, 105(2), p. 389.

[22] Frohn, A., and Roth, N., 2000. "Dynamics of droplets."

[23] Sirignano, W. A., 2014, Progress in Energy and Combustion Science, 42, pp. 54–86.

[24] Fieberg, C., Reichelt, L., Martin, D., Renz, U., and Kneer R., 2009, International Journal of Heat and Mass Transfer, 52(15-16), pp. 3738–3746.

[25] Settles, G. S., 2006, "Schlieren and shadowgraph techniques: Visualizing phenomena in transparent media."